Zero-temperature phase diagram of the second layer of ^{4}He adsorbed on graphene

M. C. Gordillo

*Departamento de Sistemas Físicos, Químicos y Naturales, Facultad de Ciencias Experimentales, Universidad Pablo de Olavide,
Carretera de Utrera km 1, 41013 Sevilla, Spain*

J. Boronat

Departament de Física i Enginyeria Nuclear, Universitat Politècnica de Catalunya, Campus Nord B4-B5, 08034 Barcelona, Spain

The phase diagram at zero temperature of ^{4}He adsorbed on a helium incommensurate triangular solid on top of a single graphene sheet has been obtained using the diffusion Monte Carlo method. We have found that, in accordance with previous experimental and simulation results for graphite, the ground state of ^{4}He on this setup is a liquid that, upon compression, transforms into a triangular solid. To define the stability limits of both liquid and solid phases, we considered not only the adsorption energies of the atoms located on the second layer but the average energy of the atoms in both layers. Our results show that the lower density limit for a stable liquid in the second layer is 0.163 ± 0.005 Å^{-2} and that the lower limit for the existence of an incommensurate solid on the second layer is 0.186 ± 0.003 Å^{-2}. Both values are in overall agreement with the results of torsional oscillator experiments and heat capacity measurements on graphite. The 4/7 and 7/12 registered solids are found to be metastable with respect to triangular incommensurate arrangements of the same density.

　　　　　　　PACS number(s): 68.65.Pq, 67.25.dp, 02.70.Ss, 05.30.Jp

I. INTRODUCTION

Graphene is a novel form of carbon in which the atoms are located in the vertices of a two-dimensional honeycomb lattice.[1,2] This means that it could be thought of as the result of isolating each of the multiple layers that conforms a graphite structure, or as the flat counterpart of a carbon nanotube. In principle, graphene could be used as a gas adsorbent at very low temperatures in the same way as graphite (see for instance Ref. 3), or a carbon nanotube,[4] but up to now this has not been experimentally realized. The only studies on that surface are computer simulations.[5–8] All these works consider only the first layer of a quantum species (^{4}He, H$_2$) adsorbed on its surface, and their results indicate that graphene behaves as an adsorbent basically like graphite. The main difference is an almost constant offset of the binding energy per particle due to the presence of more carbon atoms in the graphite case.

In this paper, we are interested in the behavior of ^{4}He adsorbed on top of a helium triangular solid resting on a single graphene layer, i.e., in the second layer of ^{4}He on graphene. Since there are not experimental results on graphene, the only data to compare to will be the heat capacity,[9,10] third sound,[11] and torsional oscillator[12,13] measurements on graphite. The same applies to previous Green's function Monte Carlo (GFMC)[14] and path integral Monte Carlo (PIMC)[15–17] calculations on this system: All are performed for ^{4}He on graphite. One of our aims in this paper is to check if the phase diagrams on graphite are similar to those on graphene, as happened to the first layer of helium.

The picture that emerges from experimental and simulation results of ^{4}He on graphite indicates that, when the total density increases, there is a promotion to a second layer. This transition density was found to be in the range 0.115–0.12 Å^{-2} in neutron[18] and heat capacity measurements,[9,10,19] in good agreement with PIMC[17] (0.1140 ± 0.0003 Å^{-2}), and GFMC[14] (between 0.115 and 0.118 Å^{-2}) calculations. From there up, according to heat capacity data,[10] there is a stable liquid phase

in the range 0.16–0.19 Å^{-2}; this interval includes the one inferred from torsional oscillator experiments[12,13] (0.174–0.19 Å^{-2}). From 0.19 Å^{-2} up, an incommensurate solid is found, whose stability limit ends with the helium promotion to the third layer at densities ranging from 0.204 Å^{-2} (Refs. 11–13) to 0.212 Å^{-2} (Ref. 10). Experimental[10] and theoretical[15,16] data also suggest the existence of a commensurate 4/7 phase (registered with the first layer incommensurate solid) on this second layer, analogous to what happens to ^{3}He on the same substrate,[20] even though other calculations[17] contradict these findings. The existence of a 7/12 registered solid was also studied in Ref. 17 and found unstable.

All previous simulations that went beyond considering the second layer of ^{4}He on graphite as a purely two-dimensional system were PIMC calculations.[15–17] The study of the phase boundaries with PIMC is difficult since to check the relative stability of the different atom arrangements free energy calculations[21] have to be done, and the primary output of finite temperature calculations is the energy, not the free energy. On the other hand, the diffusion Monte Carlo (DMC) technique appears to be ideally suited for that purpose. First, it is a ground-state method which works at $T = 0$. Second, it allows us to introduce at will the particular phase or set of phases we are interested in through an appropriate importance sampling. One arrangement is preferred over another with the same density if the energy per particle in the former is smaller than in the latter. This simple prescription, together with the use of double tangent Maxwell constructions, permits us to establish with precision the stability boundaries of the different phases proposed.

In this paper, we report the results of performing different series of DMC calculations to obtain the ground-state phase diagram of the second layer of ^{4}He adsorbed on graphene. The next section is devoted to the description of the technique and approximations used to do so. Section III shows the results obtained, leaving the conclusions for Sec. IV.

II. METHOD

Our microscopic study of the second layer of ^{4}He on graphene is based on the DMC method. Nowadays, DMC is a standard tool that allows for an exact calculation of ground-state properties of boson systems, within some statistical uncertainties, by solving stochastically the multiparticle Schrödinger equation.[22] In order to reduce the variance to a manageable level, one introduces the usual importance sampling strategy through a guided diffusion process. The drift force is intended for focusing the sampling to regions where one reasonably expects that the wave function of the system is large. Technically, this is implemented by introducing a guiding wave function that avoids interparticle distances smaller than the core of the interactions, localizes particles close to the adsorbing surface, and fixes the phase (liquid or solid) of the system. The model we have used in the present study is

$$\Phi(\mathbf{r}_1, \ldots, \mathbf{r}_N) = \Phi_J(\mathbf{r}_1, \ldots, \mathbf{r}_N)\Phi_1(\mathbf{r}_1, \ldots, \mathbf{r}_{N_1})$$
$$\times \Phi_2(\mathbf{r}_{N_1+1}, \ldots, \mathbf{r}_N), \qquad (1)$$

where N is the total number of atoms and N_1 the fraction of them located in the first layer. The first term is a Jastrow factor that accounts for the ^{4}He-^{4}He dynamical correlations induced by their interparticle interaction,

$$\Phi_J(\mathbf{r}_1, \ldots, \mathbf{r}_N) = \prod_{1=i<j}^{N} \exp\left[-\frac{1}{2}\left(\frac{b}{r_{ij}}\right)^5\right]. \qquad (2)$$

In Eq. (2), b is a variational parameter that has been already optimized in previous simulations of ^{4}He in various setups[5,22,23] and found to be 3.07 Å. The second and third terms in the r.h.s. of Eq. (1) are introduced to describe approximately the first and second layer, respectively. Explicitly,

$$\Phi_1(\mathbf{r}_1, \ldots, \mathbf{r}_{N_1}) = \prod_{i=1}^{N_1} \Psi_1(z_i) \prod_{i,I=1}^{N_1} \exp\left\{-a_1\left[(x_i - x_I^{(1)})^2\right.\right.$$
$$\left.\left. + (y_i - y_I^{(1)})^2\right]\right\}, \qquad (3)$$

$$\Phi_2(\mathbf{r}_{N_1+1}, \ldots, \mathbf{r}_N) = \prod_{i=N_1+1}^{N} \Psi_2(z_i) \prod_{i,I=N_1+1}^{N} \exp\left\{-a_2\left[(x_i - x_I^{(2)})^2\right.\right.$$
$$\left.\left. + (y_i - y_I^{(2)})^2\right]\right\}. \qquad (4)$$

In Φ_1, the Gaussian terms define the triangular solid that comprises the first layer, where the coordinate set $(x_I^{(1)}, y_I^{(1)})$ are the lattice sites; these positions can be varied to consider different densities. The optimal value for the parameter a_1, that defines the strength of the localization factor, has been taken from DMC simulations of the first layer.[5] As in that work, the parameter a_1 is varied linearly with density between $a_1 = 0.30$ Å^{-2} at 0.08 Å^{-2} and $a_1 = 0.77$ Å^{-2} for 0.128 Å^{-2}. On the other hand, $\Psi_1(z)$ is the solution of the one-dimensional Schrödinger equation for a single atom moving perpendicularly to the graphene plane with a potential that is the averaged out version in the z axis of all the Lennard Jones interactions between all the carbon atoms and the ^{4}He atom. This is exactly what was made in Refs. 5 and 14.

Φ_2 in Eq. (4) accounts for the properties of the second layer. The function $\Psi_2(z)$ is the solution of the Schrödinger equation for a single atom on top of both graphene and a fixed helium layer of density 0.11 Å^{-2}. It has a maximum at a distance of 5.59 Å from the position of the graphene layer, and it has been used for all the calculations involving the different phases on the second layer. As in the first layer, the different solid phases have been modeled by defining their corresponding lattice positions $(x_I^{(2)}, y_I^{(2)})$ and by their a_2 parameters, obtained variationally for each considered density. This optimization leads to the same density dependence as the one obtained for the first layer. If the upper layer is a liquid, $a_2 = 0$.

The helium-helium interactions in both layers were modeled by an Aziz potential,[24] and the carbon-helium ones by a Lennard-Jones interaction.[25] All the carbon atoms in the graphene layer have been considered individually, i.e., full corrugation effects have been taken into account. We also tested an alternative form of the carbon-helium interaction that is explicitly anisotropic,[26] and the results were found to be very similar to the ones obtained with the isotropic Lennard-Jones potential. The only difference was a decrease in the energy per particle in the range 0.5–1 K, depending on the density of the particular arrangement considered. The stability limits of the phases remained independent of this choice for the pair carbon-helium potential because the second layer is much less influenced by corrugation effects than the first one.

When the second layer phase is liquid or a registered structure, a rectangular simulation cell, defined by the triangular solid that comprised the underlying helium sheet, is used. However, if the upper structure is an incommensurate arrangement, there is in principle a mismatch between the first and second crystallographic structures. To solve the problems created by this situation, we define independent simulation cells on the first and second layer. Then, for a given rectangular simulation cell for the first layer, we consider all the interactions between the atoms in that cell and the particles on the second layer that are within a given distance r_{cut} from any of the helium atoms underneath. To do so, we use the positions of all the atoms in that layer and their respective second layer periodic boundary conditions images. Working in this way, we can consider any upper or lower densities, not needing to confine ourselves to quasicommensurate arrangements.[16] In all calculations, all the positions of the particles, both in the first and second layer, were allowed to move during the simulations, i.e., zero-point motion was considered for all helium atoms.

III. RESULTS

A. Second layer promotion

The first concern about the second layer of a given adsorbate is the total density at which that layer starts to form. One way to answer this question is to determine the chemical potential of a single atom adsorbed on top of a helium layer and compare it to the same parameter for the atoms that constitute the lower solid helium layer. The promotion will take place at the particular first layer density at which both chemical potentials are equal. This is the procedure used previously in graphite,[14,17] giving a first layer density between 0.114 and 0.118 Å^{-2}. Our approach relies on the same theoretical grounds but it is slightly different
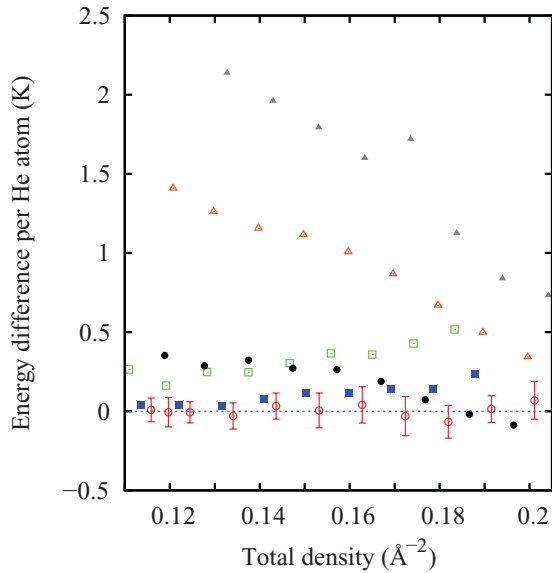
FIG. 1. (Color online) Relative energy per particle values with respect to a fourth-order polynomial fit to the energy per particle of an structure in which the underlying solid has a density of 0.115 Å^{-2} (dashed line). From top to bottom, we show liquid layers on top of solids of 0.1225 Å^{-2} (full triangles), 0.12 Å^{-2} (open triangles), 0.1175 Å^{-2} (full circles), 0.115 Å^{-2} (real simulation results minus the values obtained from the fit at the same densities, open circles), 0.1125 Å^{-2} (full squares), and 0.11 Å^{-2} (open squares).

from a technical point of view: to determine the lowest second layer density for which a liquid phase is stable, we perform a Maxwell construction between the simulation results for the energy per particle in a one-layer setup and the ones for an arrangement with a liquid on top of a quasi-two-dimensional solid.

The first step in the present case is to determine which is the density of the underlying solid for which the energy per atom (including both layers) is the lowest. This can be done with the help of Fig. 1. There, we plot the relative energy per particle for different first layer solids as a function of the total density. We have used relative values instead of absolute ones due to the small energy differences between the possible configurations. We choose as reference values for each density the ones for an upper liquid in which the first solid helium layer has a fixed density of 0.115 Å^{-2}. What we present in Fig. 1 is the difference between the energy per atom for a given structure and a fourth-order polynomial fit to the values corresponding to solid density 0.115 Å^{-2}. This means that if the energy per particle for a particular arrangement is lower than the one for a liquid on top of a solid of 0.115 Å^{-2} with the same total density, it will be represented by a negative value in Fig. 1 and vice versa. The real simulation results for the reference setup are displayed as open circles with their error bars, to be compared with the dashed line that indicates the fit to them. The error bars for other structures and densities are similar to those and not displayed for clarity. What we can see is that the relative energies for all other setups, with underlying solid densities ranging from 0.11 (open squares) to 0.1225 Å^{-2} (full triangles), are always greater than zero, i.e., the system with the smallest energy is a liquid on top of a triangular solid of density
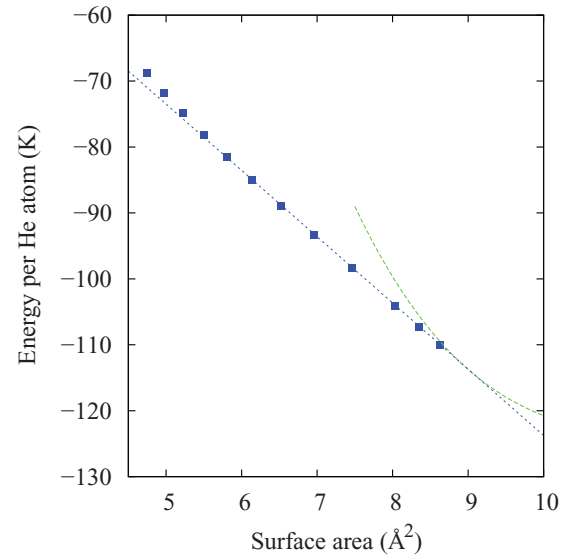

FIG. 2. (Color online) Energy per particle for a structure with a single layer triangular solid (dashed line) and a second layer liquid on top of a solid of density 0.115 Å^{-2} (full squares) versus the inverse of the total helium density. The common tangent of a Maxwell construction is represented by a dotted line.

0.115 Å^{-2}. The only possible exception would be a liquid with $\sigma > 0.0725$ Å^{-2} on top of a solid of density 0.1175 Å^{-2} (a total density $\sim$0.19 Å^{-2}). However, at these densities the liquid phase on the second layer is no longer stable (see discussion below). We can see also that in the range 0.11–0.1175 Å^{-2} the energy differences for the full structures are very small, even lower than 1 K, pointing to the difficulty of a precise determination of the promotion density.

Once we have established from first principles which first layer solid to use, one should perform a double-tangent Maxwell construction to determine the lowest stability limit for a second layer liquid after helium promotion.[27] The necessary data are displayed in Fig. 2. There, we show a third-order polynomial fit to the energy per particle of single layer solids of different densities, taken from Ref. 5 (dashed line), together with the present simulation results (full squares) corresponding to liquids on top of a first layer of density 0.115 Å^{-2}. The dotted line defines the common tangent for the equilibrium configurations in the one and two layer structures. This means that the first layer solid is stable up to the surface area at which the energy per particle curve has the same slope as the dotted line, and the second layer liquid starts at the last density at which its curve also has that slope. The intermediate points correspond to inhomogeneous second layer liquid arrangements whose energies per particle are the density weighted averages of the energies of the structures in equilibrium at the transition. From Fig. 2, we can state that the approximate density of the one layer solid in equilibrium with the liquid is 0.113 ± 0.001 Å^{-2}, corresponding to a surface area of $\sim$8.8–8.9 Å^2, and that the pressure (minus the slope of the Maxwell construction line) at which the first order transition takes place is $\sim$10.06 K/Å^2. That density corresponds to the helium promotion to the second layer and is compatible with those of previous simulations[14,17] and with neutron diffraction experiments[18] on graphite. However, this
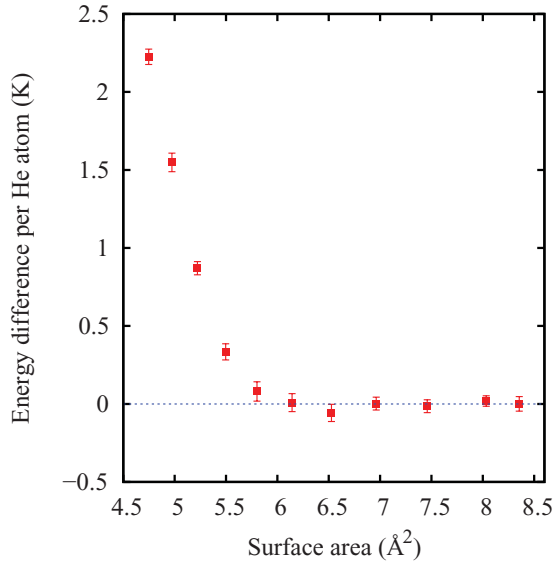
FIG. 3. (Color online) Energies per particle from the simulation results displayed in Fig. 2 (full squares) minus the corresponding values obtained from the double tangent line, here represented as a dashed line.

value is somehow smaller than the one inferred from some heat capacity measurements[9,10] (0.12 Å^{-2}) on the same substrate, even though it is compatible with others.[19] Our result points to the prediction that the second layer promotion of ^{4}He on graphene takes place at the same density as on graphite.

B. Second layer liquid

The lower density limit for the second layer liquid is then the last point for which the simulation results share the common tangent. This is difficult to see in Fig. 2, and for this reason we have displayed the same data in a slightly different form in Fig 3. There, we show the difference between the energy per particle obtained from the simulations and the one obtained from the Maxwell construction line. Obviously, that difference is zero if the points are on top of that line: The smaller surface area that fulfills this prescription is 6.14 Å^2, that corresponds to a density of 0.163 ± 0.005 Å^{-2}. The error bar is estimated as half of the distance between the simulated points. This value compares favorably with the experimental data of Greywall[9,10] ($\sim$0.16 Å^{-2}), but is slightly smaller than the one obtained from torsional oscillator experiments by Crowell and Reppy in graphite ($\sim$0.17 Å^{-2}).[12,13] If we subtract the density of the first layer, the remaining density, 0.048 ± 0.005 Å^{-2} is also compatible with the strictly two-dimensional calculations of Refs. 21 and 23 ($\sim$0.043 Å^{-2} in both cases), and with PIMC results on graphite,[17] in which a similar value is given (0.046 Å^{-2}). In the latter case, the full three-dimensional structure was used, with an underlying solid in which the atomic zero-point motion was taken into account. However, in Ref. 17 no prediction about the density of the first layer is given, stating only that the location of the liquid equilibrium density was independent of that value. This is probably due to the small energy differences between structures with different underlying solid densities, as commented above. For second layer densities between 0 and 0.048 Å^{-2}, the second layer

liquid is unstable, and the system will separate in puddles of 0.048 Å^{-2} and enough empty space to average any density considered in this range.

If we consider only the energy per particle of the helium atoms in the second layer, we have the isotherm displayed in Fig. 4. There, we show the simulation results (open squares, left scale) together with a third-order polynomial fit that allows us to estimate that the minimum energy per particle is $-22.14 \pm$ 0.04 K for an equilibrium density of 0.045 ± 0.001 Å^{-2}. This density is a bit lower but compatible with the result quoted in the previous paragraph (0.048 ± 0.005 Å^{-2}). At least, part of the difference could be ascribed to the behavior of the ^{4}He atoms closest to the graphene substrate: far from being constant, the energy per particle decreases up to 0.8 K per particle due to the presence of the upper liquid layer. This means that to describe this system probably one has to take into account both layers. The infinite-dilution limit for the second layer at this underlying density is -21.53 ± 0.01 K. Previous simulation results on graphite report values of -29.6 ± 0.3 K (Ref. 17), and -29.8 K for slightly smaller underlying helium densities. This implies an increase in the binding energy of a single atom on the top layer from graphene to graphite of about 40%, versus a similar 10% growing for a single atom on bare graphene or graphite.[5] On the other hand, the energy difference between the infinite-dilution limit and the energy minimum is -0.61 ± 0.04 K, to be compared to ~ -0.9 K of the pure two-dimensional calculation with the same potential.[23] This means that the second layer liquid is not fully two dimensional, as can be seen also with the help of Fig. 5. There, we show the density profiles in a direction perpendicular to the graphene layer of both layers in two arrangements: the lowest liquid density limit (full line), and an upper layer solid of 0.07 Å^{-2} on top of a triangular solid of 0.1175 Å^{-2} (dashed line). Far from being delta functions, both layers display a sizable width, that is obviously larger for the top one.

C. Second layer solid

If more helium is added, the system evolves to form an incommensurate second layer solid. The lower density limit of the layer solid at the transition can be obtained with the help
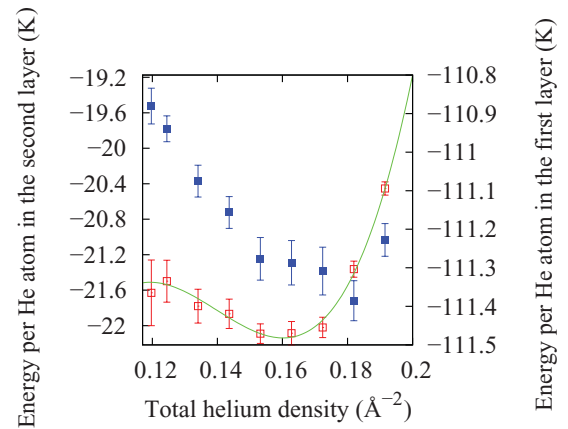

FIG. 4. (Color online) Energy per particle of ^{4}He in the first (full squares, right scale) and second (open squares, left scale) layer for a liquid phase on top of a solid of density 0.115 Å^{-2}.
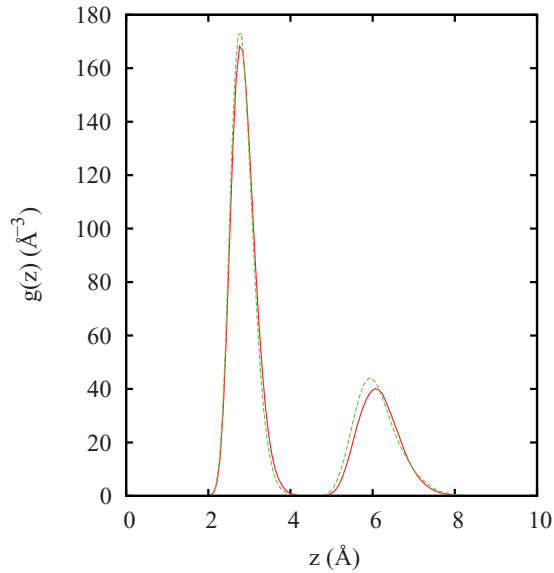
FIG. 5. (Color online) Density profiles as a function of the distance perpendicular to the graphene layer for a second layer liquid with total density 0.163 Å^{-2} (solid line) and a double solid of total density of 0.1875 Å^{-2} (dashed line). In the latter case, the density of the underlying solid is 0.1175 Å^{-2}.

of Fig. 6. In this figure, we display as symbols the energies per particle for different solid arrangements as a function of the surface area. The error bars are of the size of the symbols and not shown for simplicity. The lower value in the x axis corresponds to the smaller experimental density at which a promotion to the third layer has been reported.[12,13] The dashed line is the fourth-order polynomial fit to the simulation data for a liquid phase, already used in Fig. 1. The Maxwell construction between this structure and a second layer solid on top of a triangular solid with a density of 0.1175 Å^{-2} (full squares) is represented by the dotted line, while the full curve is a fit to those data. From Fig. 6 it is clear that the upper equilibrium density for a second layer liquid is around 0.170 ± 0.005 Å^{-2}, derived from a surface area of ∼5.9 Å^2. We can also see that the last of the open squares, representing an incommensurate top solid on a first layer arrangement of density 0.115 Å^{-2}, is on top of the common tangent line. The upper surface limit, according to the Maxwell construction, is comprised between densities 0.185 and 0.1875 Å^{-2}. The first value corresponds to an incommensurate solid of 0.07 Å^{-2} on top of a 0.115 Å^{-2}, and the second, to an upper arrangement of the same density but on top of a first layer solid of 0.1175 Å^{-2}. Unfortunately, the simulation results do not allow us to discriminate between these two possibilities. The upper layer density is slightly smaller than the result obtained in previous PIMC calculations[17] (0.076 ± 0.002 Å^{-2}) and to a zero-temperature DMC estimation of the melting density in a strictly two-dimensional crystal (0.075 ± 0.001 Å^{-2}).[28] From the difference in the total density, we can estimate than the error bar for the upper density limit is 0.0025 Å^{-2}, i.e., our estimation for the total density is 0.186 ± 0.003 Å^{-2}. This density is in reasonable agreement with the value of 0.19 Å^{-2} that heat capacity data[9,10] shows for the appearance of a *commensurate* solid, and with the experimental value of
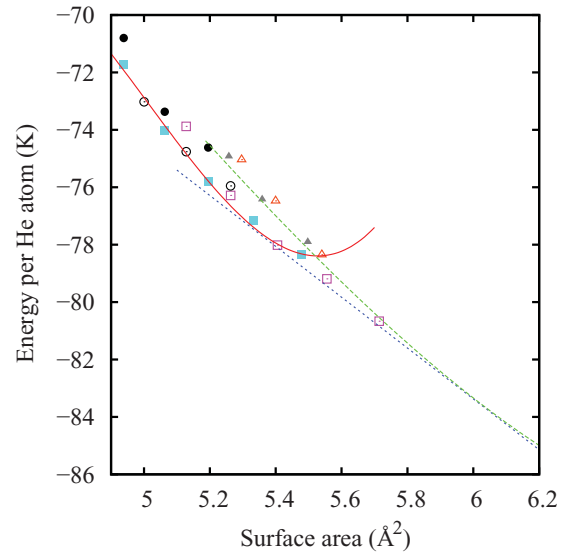

FIG. 6. (Color online) Energies per particle for different incommensurate solids versus the inverse of the total density. The first layer densities are 0.115 Å^{-2} (open squares); 0.1175 Å^{-2} (full squares); 0.12 Å^{-2} (open circles), and 0.1225 Å^{-2} (full circles). The dashed line represents a fourth-order polynomial fit to a second layer liquid, with underlying density of 0.115 Å^{-2}, while the dotted line is the double-tangent Maxwell construction. Triangles stand for the energy per particle for two commensurate unstable arrangements on top of different first layer incommensurate solids: full triangles, 7/12 structure; open triangles, 4/7 solid.

∼0.191 Å^{-2} for the disappearance of the superfluid signal in torsional oscillator experiments,[12] both experiments on graphite. If we keep on adding helium, for total densities larger than ∼0.1950 ± 0.0025 Å^{-2}, corresponding to a surface area of 5.13 Å^2, we can see that the results for an incommensurate solid with a first layer density of 0.12 Å^{-2} (open circles) are on top of the fit corresponding to a 0.1175 Å^{-2} solid. Therefore, for this density on a different stable two layer solid phase could be possible, even though one cannot discriminate between both from energetic arguments. However, we are sure that no further compression of the first layer is possible, since the energy per helium atom for a double solid with a lower density of 0.1225 Å^{-2} is bigger than for its 0.12 Å^{-2} counterpart (full circles in Fig. 6). Obviously, none of these changes can be described by a two-dimensional model since the density of the underlying solid is different for the possible phases in equilibrium.

To complete the study of the second layer phase diagram, we have analyzed the possible existence of commensurate structures on top of the first layer triangular ^{4}He solids. The existence of a $\sqrt{7} \times \sqrt{7}$ phase, equivalent to the 4/7 commensurate arrangement found experimentally[20] in ^{3}He, has been theoretically[15,16] and experimentally[10] proposed for graphite. However, a previous calculation of helium on graphite[17] indicated that the theoretical stability of this phase was motivated by the consideration of a completely frozen first layer solid. This conclusion is supported by our data displayed in Fig. 6 as open triangles. The three points shown in the figure correspond to 4/7 structures on top of first layers of densities 0.115, 0.1175, and 0.12 Å^{-2}; all of them are unstable with

respect to a second layer liquid of the same total density. The same can be said of the possibility of a 7/12 phase. The three full triangles in Fig. 6 represent the energies for that lattice on top of the same first layer solids as in the previous case. In all cases, the registered solids are also unstable with respect to the second layer liquid.

IV. CONCLUSIONS

Our microscopic results show that ^{4}He promotion to a second layer on graphene starts at a first layer density of 0.113 ± 0.001 Å^{-2}. This phase is in equilibrium with a second layer liquid of density 0.048 Å^{-2} on top of an underlying solid of 0.115 Å^{-2}. Upon addition of more helium, the second layer liquid undergoes a first order phase transition to an incommensurate second layer solid of density 0.070 Å^{-2} on top of either a 0.115 or a 0.1175 Å^{-1} layer (both options are equally possible within the accuracy of our calculations). Therefore, the stability window for a second layer homogeneous liquid is 0.163–0.170 Å^{-2}, and that from this last density up, there should be a coexistence zone with a two-solid structure whose maximum total density is 0.1875 Å^{-2}. This means that from 0.170 Å^{-2} on, the upper layer should be formed by patches of superfluid liquid together with incommensurate solid domains. Those liquid patches would be responsible for the torsional oscillator signal seen up to 0.191 Å^{-2} in graphite. No indication of the width of the transition region can be deduced from the heat capacity measurements on the same substrate. We are only aware of a value 0.0031 Å^{-2} reported in PIMC calculations[21] at $T = 0.25$ K, five times smaller than the difference estimated here, between 0.185 and 0.170 Å^{-2}. Even though this is at best a crude approximation, it is clear that experimentally a transition region should exist, and it should start at densities lower than the last for which a superfluid signal can be obtained. Our results also suggest that the peak that appears in the heat capacity data of Ref. 10 at 0.19 Å^{-2} could be ascribed to a transition to an incommensurate solid, not to a commensurate one.

Our simulation results suggest also an explanation for the displacement of the transition peak from 0.19 to 0.197 Å^{-2} in heat capacity data: It could be the result of a further compression of the first layer solid. However, in our data, that compression is smaller than that measured in Refs. 9 and 10: a theoretical maximum density of 0.12 Å^{-2} instead of the 0.127 Å^{-2} density of the experimental data, a 6% difference. The experimental difference between the total density at the second layer promotion (0.12 Å^{-2}) and that of the underlying solid near second layer compression (0.127 Å^{-2}) is also 6%. The equivalent values obtained from our simulations are 0.113 and 0.12 Å^{-2}, also a 6% change.

[1] K. S. Novoselov, A. K. Geim, S. V. Morozov, D. Jiang, Y. Zhang, S. V. Dubonos, and I. V. Grigorieva, and A. A. Firsov, Science **306**, 666 (2004).

[2] K. S. Novoselov, D. Jiang, F. Schedin, T. J. Booth, V. V. Khotkevich, S. V. Morozov, and A. K. Geim, PNAS **102**, 10451 (2005).

[3] L. W. Bruch, M. W. Cole, and E. Zaremba, *Physical adsorption: forces and phenomena* (Oxford University Press, Oxford, 1997).

[4] Z. Wang, J. Wei, P. Morse, J. G. Dash, and O. E. Vilches, and D. H. Cobden, Science **327**, 552 (2010).

[5] M. C. Gordillo and J. Boronat, Phys. Rev. Lett. **102**, 085303 (2009).

[6] M. C. Gordillo and J. Boronat, Phys. Rev. B **81**, 155435 (2010).

[7] M. C. Gordillo, C. Cazorla, and J. Boronat, Phys. Rev. B **83**, 121406(R) (2011).

[8] M. C. Gordillo and J. Boronat, Phys. Rev. B **84**, 033406 (2011).

[9] D. S. Greywall and P. A. Busch, Phys. Rev. Lett. **67**, 3535 (1991).

[10] D. S. Greywall, Phys. Rev. B **47**, 309 (1993).

[11] G. Zimmerli, G. Mistura, and M. H. W. Chan, Phys. Rev. Lett. **68**, 60 (1992).

[12] P. A. Crowell and J. D. Reppy, Phys. Rev. Lett. **70**, 3291 (1993).

[13] P. A. Crowell and J. D. Reppy, Phys. Rev. B **53**, 2701 (1996).

[14] P. A. Whitlock, G. V. Chester, and B. Krishnamachari, Phys. Rev. B **58**, 8704 (1998).

[15] M. E. Pierce and E. Manousakis, Phys. Rev. Lett. **81**, 156 (1998).

[16] M. E. Pierce and E. Manousakis, Phys. Rev. B **59**, 3802 (1999).

[17] P. Corboz, M. Boninsegni, L. Pollet, and M. Troyer, Phys. Rev. B **78**, 245414 (2008).

[18] K. Carneiro, L. Passell, W. Thomlinson, and H. Taub, Phys. Rev. B **24**, 1170 (1981).

[19] S. E. Polanco and M. Bretz, Phys. Rev. B **17**, 151 (1978).

[20] H. Fukuyama, J. Phys. Soc. Jpn. **77**, 111013 (2008).

[21] M. C. Gordillo and D. M. Ceperley, Phys. Rev. B **58**, 6447 (1998).

[22] J. Boronat and J. Casulleras, Phys. Rev. B **49**, 8920 (1994).

[23] S. Giorgini, J. Boronat, and J. Casulleras, Phys. Rev. B **54**, 6099 (1996).

[24] R. A. Aziz, F. R. W. McCourt, and C. C. K. Wong, Mol. Phys. **61**, 1487 (1987).

[25] G. Stan and M. W. Cole, Surf. Sci. **395**, 280 (1998).

[26] W. E. Carlos and M. W. Cole, Surf. Sci. **91**, 339 (1980).

[27] D. Chandler, *Introduction of modern statistical mechanics* (Oxford University Press, Oxford, 1987).

[28] C. Cazorla, G. E. Astrakharchik, J. Casulleras, and J. Boronat, J. Phys.: Condens. Matter **22**, 165402 (2010).